An Observational Constraint on Aviation-Induced Cirrus From the COVID-19-Induced Flight Disruption

Ruth A. R. Digby, Nathan P. Gillett, Adam H. Monahan, Jason N. S. Cole

October 2021

AGU ADVANCING EARTH AND SPACE SCIENCE

Geophysical Research Letters®

RESEARCH LETTER
10.1029/2021GL095882

Special Section:
The COVID-19 pandemic: linking health, society and environment

An Observational Constraint on Aviation-Induced Cirrus From the COVID-19-Induced Flight Disruption

Ruth A. R. Digby[1], Nathan P. Gillett[2], Adam H. Monahan[1], and Jason N. S. Cole[2]

[1]School of Earth and Ocean Sciences, University of Victoria, Victoria, BC, Canada, [2]Canadian Centre for Climate Modelling and Analysis, Environment and Climate Change, Victoria, BC, Canada

Key Points:

- Aviation reductions during COVID-19 provide an opportunity to test the impact of aviation on cirrus cloud and diurnal temperature range
- Neither variable exhibits a detectable large-scale response in satellite observations
- Comparison with previous model analyses of contrail cirrus suggests that warming by aviation-induced cirrus may have been overestimated

Supporting Information:

Supporting Information may be found in the online version of this article.

Correspondence to:

R. Digby,
digbyr@uvic.ca

Citation:

Digby, R. A. R., Gillett, N. P., Monahan, A. H., & Cole, J. N. S. (2021). An observational constraint on aviation-induced cirrus from the COVID-19-induced flight disruption. *Geophysical Research Letters*, *48*, e2021GL095882. https://doi.org/10.1029/2021GL095882

Received 10 SEP 2021
Accepted 27 SEP 2021

Abstract Global aviation dropped precipitously during the Covid-19 pandemic, providing an unprecedented opportunity to study aviation-induced cirrus (AIC). AIC is believed to be responsible for over half of aviation-related radiative forcing, but until now, its radiative impact has only been estimated from simulations. Here, we show that satellite observations of cirrus cloud do not exhibit a detectable global response to the dramatic aviation reductions of spring 2020. These results indicate that previous model-based estimates may overestimate AIC. In addition, we find no significant response of diurnal surface air temperature range to the 2020 aviation changes, reinforcing the findings of previous studies. Though aviation influences the climate through multiple pathways, our analysis suggests that its warming effect from cirrus changes may be smaller than previously estimated.

Plain Language Summary Global air traffic decreased rapidly during the Covid-19 pandemic. This perturbation provides an opportunity to test the influence of aviation on cirrus cloud cover and on the contrast between daytime and nighttime surface air temperatures. We find that, despite the very large reduction in air traffic, neither cirrus cover nor temperature ranges changed by enough to be detectable relative to the year-to-year variability of natural cirrus. Comparing the satellite observations to previous model-simulated aviation cirrus, we determine that any aviation-induced change in cirrus would have a much smaller magnitude than would be inferred from climate model simulations. These results suggest that the warming effect of cirrus clouds produced by aircraft may be smaller than previously believed.

1. Introduction

Aviation is responsible for an estimated 3.5% of anthropogenic effective radiative forcing (ERF) (Lee et al., 2021), a number that has been growing rapidly as air traffic has increased over recent decades. Of this forcing, the largest—and most uncertain—component is the contribution from contrail cirrus, which is estimated to make up ~55% of the total aviation forcing and was calculated at 57 (17, 98) mW/m^2 for 2018 in a recent multimodel synthesis (Lee et al., 2021).

Contrail cirrus consists of both linear contrails, which form behind aircraft, and the artificial cirrus cloudiness formed when these linear contrails disperse. Because aircraft emission plumes may be temporarily supersaturated with respect to ice (Minnis et al., 2004), contrails can form in conditions where natural cirrus cannot and therefore have the potential to substantially impact regional high-level cloudiness (Burkhardt & Kärcher, 2011; Sassen, 1997). High-level cloud is also affected by the aerosols emitted by aircraft, which can serve as ice nuclei; the ice nucleation efficiency of black carbon, in particular, remains uncertain (Karcher et al., 2007; Kärcher et al., 2021; Voigt et al., 2021). Finally, the formation of contrail cirrus can compete with natural cirrus for water vapor, reducing the formation of the latter (Burkhardt & Kärcher, 2011). In this work, we will refer to the combination of these effects as aviation-induced cirrus (AIC). Like natural cirrus, the radiative impact of AIC is dominated by its longwave effect and is expected to decrease the diurnal surface air temperature range (DTR) (Sassen, 1997; Travis & Changnon, 1997; Travis et al., 2002).

Because of its large radiative impact and short lifetime, AIC is a popular target for mitigation strategies aimed at reducing the climate impact of aviation (see, e.g., overview in Kärcher, 2018). One such strategy is navigational avoidance or the diversion of flight paths away from regions where contrails are likely to form (Grewe1 et al., 2017; Kärcher, 2018; Rosenow et al., 2018). However, the efficacy of this approach hinges on contrail cirrus having a substantially larger radiative forcing than other aviation sources such as CO_2,

since rerouting will result in a longer flight track and correspondingly higher emissions. Therefore, there is a substantial interest from both scientific and policy-making communities in a detailed understanding of the radiative impact of AIC.

This radiative impact is extremely difficult to constrain. Once linear contrails disperse into contrail cirrus, they become indistinguishable from natural cirrus, precluding observational studies over the majority of their evolution (Burkhardt et al., 2010; Kärcher, 2018). Possible influences of climate change or changes in other sources of anthropogenic aerosols make it difficult to isolate the impacts of the long-term increase in aviation. Simulating AIC requires a detailed representation of microphysics and particle characteristics (Bock & Burkhardt, 2016b; Kärcher, 2018; Kärcher et al., 2009), and radiative transfer calculations have proven to be sensitive to models' horizontal, vertical, and temporal resolution (Lee et al., 2021; Myhre et al., 2009) as well as the choice of the radiative transfer scheme itself (Myhre et al., 2009). Indirect sources of AIC (the soot-cloud effect and impacts of AIC on natural cirrus) are even more poorly constrained (Burkhardt & Kärcher, 2011; Kärcher, 2018; Lee et al., 2021). For a detailed discussion of the uncertainties in simulating AIC RF, refer to Lee et al. (2021).

Given the immense challenge of simulating and observing AIC, large-scale flight groundings provide our best probe of the relationships between aviation density, cirrus cover, and DTR. The aviation reductions associated with the Covid-19 pandemic have dwarfed previous flight groundings, which were too short and too geographically limited to yield robust signals (Hong et al., 2008; Sandhu & Baldini, 2018; Travis et al., 2002). In early April 2020, the total number of flights globally fell to <40% of 2019 levels (FlightRadar24, 2020a), and by December 2020, had only recovered to ~75% (FlightRadar24, 2020b). In this work, we investigate whether these unprecedented reductions in global aviation have led to detectable changes in cirrus cover or in DTR.

2. Data

2.1. Aviation Data

Spatially resolved aviation data were purchased from the global flight tracking service FlightRadar24 (FlightRadar24, 2020c). We obtained flight tracks for all recorded flights on every second Friday from January through July of 2019 and 2020, corresponding to 15 days in each year. Only 30 days' data were purchased for reasons of cost, but the days were selected days to center around the period of the greatest aviation change. Our selection matched the days of the week, rather than calendar dates, between 2019 and 2020 due to the weekly cycle in the number of flights.

We interpolate these flight tracks to a $1° \times 1°$ spatial grid and 30-s temporal grid, filtering by altitude ($z >$ 18,000ft/5,486m) to include only the flights most likely to form contrails. The resulting flight density distribution is then scaled to areal density (flights per square km). Aviation anomalies are expressed as differences between mean daily aviation densities of particular months in 2020 and 2019. The March-April-May (MAM) mean anomaly is shown in Figure S1a.

We additionally construct a 21-year aviation time series using publicly available data from Airlines for America (A4A) (Airlines for America, 2021). We quantify aviation in terms of total kilometers flown, since this metric is the most physically relevant for contrail formation; expressing aviation in terms of annual aircraft departures yields similar results shown in the Supporting Information S1. In both cases, data correspond to passenger and cargo aircraft and are only available through 2019.

Although data on total aircraft kilometers flown in 2020 are not readily available, we utilize the facts that (a) there has been a roughly linear relationship between total aircraft kilometers and assigned seat kilometers (AKSs) for the past decade (Airlines for America, 2021), and (b) in 2020, ASKs fell 68.1% over 2019 levels (IATA Pressroom, 2021). We thus obtain a value for aircraft kilometers in 2020 by scaling the kilometers flown in 2019 by a factor of $(1 - 0.681)$.

2.2. Cirrus Data

Cirrus fractions are taken from the Moderate Resolution Imaging Spectroradiometer (MODIS) instruments on the satellites Aqua and Terra (King et al., 2013; Platnick et al., 2017). Aqua and Terra have equatorial overpasses at 1:30 a.m./pm and 10:30 a.m./pm local time, respectively.

We use the product Cirrus_Fraction_Infrared_FMean from the monthly gridded products MOD08_M3 (Terra) and MYD08_M3 (Aqua), which have 1° × 1° spatial resolutions (King et al., 2013). Anomalies are expressed relative to a linear trend fit to the available historical data and are calculated individually for each grid cell. Data are available for Terra from February 2000 and for Aqua from July 2002; Aqua's MAM and annual (ANN) means are computed for 2003 onward.

The majority of our analysis utilizes the MODIS-mean cirrus fraction (i.e., the Aqua-Terra mean, spanning 2003–2020), though we show the results for the satellites individually for completeness. MAM 2020 MODIS-mean anomalies are shown in Figure S1b.

2.3. Temperature Data

Temperature data are taken from two sources: European Centre for Medium-Range Weather Forecasts (ECMWF) 5th Generation Reanalysis (ERA5) (Hersbach et al., 2018), which has the advantage of homogeneous, gridded spatial coverage, and Global Historical Climatology Network (GHCN) stations (Menne, Durre, Korzeniewski, et al., 2012; Menne, Durre, Vose, et al., 2012), which have the advantage of being instrumental station data but which have an extremely heterogeneous distribution.

ERA5 values are calculated from the data set of ERA5 hourly data on single levels from 1979 to present, which provides 2m temperature minima and maxima on a 1° × 1° spatial grid. GHCN weather station data are computed from the GHCN-D daily data set. From this data set, we select only stations from the World Meteorological Organization network, which has more than 20 days records in a given month, for every year from 2000 to 2020. These filters greatly reduce the number of available stations, but improve the reliability of the resulting anomalies. We have repeated our analysis requiring only 15 years records; although this approximately doubles the number of available stations, our conclusions are unaffected, and the change in spatial sampling with time introduces spurious signals, which can be misleading at the first glance. We therefore maintain the more rigorous selection to avoid confusion.

DTR anomalies are expressed relative to a linear trend fit to the 2000–2019 data and are individually calculated for each station or grid cell. MAM 2020 anomalies derived from the ERA5 and GHCN data are shown in Figures S1c and S1d, respectively.

3. Results

Our analysis consists of two components: first, assessing the observed response of cirrus cover and DTR to changes in aviation during 2020, relative to their typical interannual variability; and second, comparing those observations to estimates of the expected signal strength derived from the application of a statistical model to pre-existing simulations of aviation-induced cirrus. In both stages, we restrict our analysis to the region between 75 N and 75 S, as the satellite cirrus products we use are unreliable at higher latitudes (Hubanks et al., 2020). We emphasize that the results presented here describe the net effect of aviation on cirrus cloud, which includes not only the formation of contrails but also any interactions between contrail cirrus and natural cirrus or between (contrail or natural) cirrus and the aerosols emitted by aircraft.

3.1. Observed Response

As shown in Figure S1a, the 2020 aviation density anomalies—which closely resemble the typical aviation density distribution, not shown—are extremely regionalized. Aviation-induced changes in cirrus cover or DTR would therefore not be expected over large regions of the globe. To account for this, we weight our observations by the 2019 aviation density distribution, which focuses the analysis on regions where aviation is important without selecting arbitrary regions for analysis. We weight by the mean 2019 aviation density rather than by the change in aviation from 2019 to 2020 to avoid having a combination of positive and

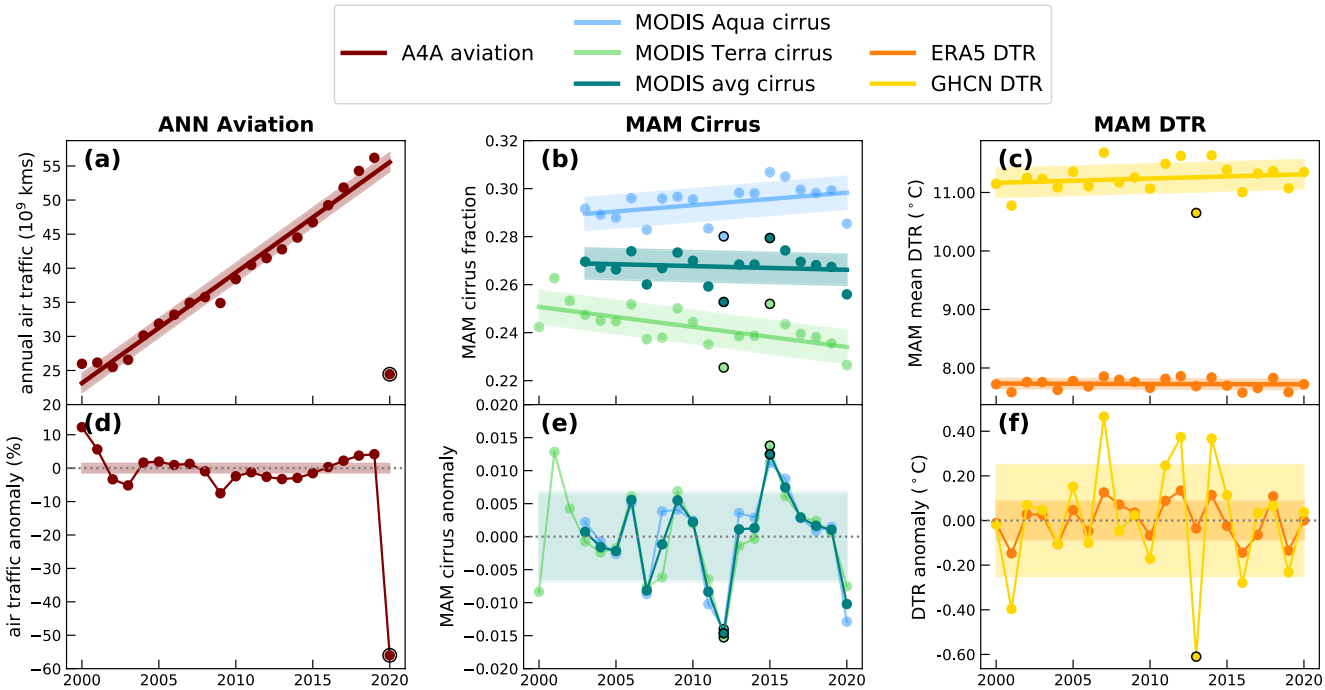

Figure 1. Evolution of air traffic, cirrus fraction, and diurnal surface air temperature range (DTR) over 2000–2020. Left (panels a, d): annual-mean aviation intensity, expressed in billions of kilometers flown. Center, right (panels b/e, cf): MAM-mean, aviation-weighted values and detrended anomalies of cirrus fraction and DTR, respectively. In all panels, solid lines show the linear trend fits, shaded regions indicate $\pm 1\sigma$, and black outlines identify anomalies that are statistically significant at the 5% level relative to the other years in the time series. The differences between DTR values calculated from ERA5 and Global Historical Climatology Network (GHCN) data in panel (c) can be ascribed to the heterogeneous spatial distribution of GHCN stations, combined with a ~2 C offset between the two data sets (Figure S2).

negative weights, as aviation levels did increase in 2020 in a small number of grid cells. The details of this calculation are described in the Supporting Information S1.

Figure 1 shows the typical values and variability of aviation, cirrus fraction, and DTR over 2000–2020. The air traffic is expressed in terms of annual kilometers flown, and the anomalies in panel (d) are expressed as a percent change relative to a linear trend fit to the 2000–2019 values. The center and right-hand columns show aviation-weighted, MAM-mean cirrus fraction and DTR, respectively; MAM is the three-month period containing the largest Covid-19-induced aviation reduction.

The center column of Figure 1 plots cirrus measurements taken from the Aqua and Terra satellites individually and the average of the two. In all three time series, the 2020 cirrus fraction anomalies are not statistically significant at the 5% level. Interestingly, the two MODIS satellites observe opposite tendencies in their cirrus data. These trends are discussed further in the Supporting Information S1.

In the right-hand column of Figure 1, orange and yellow lines correspond to DTR measurements taken from ERA5 reanalysis and GHCN weather stations, respectively. The discrepancy between their measurements is due to a combination of the heterogeneous spatial sampling of the GHCN stations and a ~2°C offset between the two data sets when sampled over the same locations (Figure S2). Despite these discrepancies, the two data sets yield the same result: aviation-weighted DTR showed no response to the Covid-19-induced aviation reductions.

The month-by-month evolution of aviation, cirrus fraction, and DTR anomalies through 2020 is examined in Figure 2. Aviation anomalies were largest in April 2020. Although cirrus fraction and DTR anomalies showed sizeable excursions around this time, these anomalies are not exceptional when compared to other excursions, which occurred later in the year when the aviation signal was much smaller. Moreover, the low cirrus fraction and high DTR observed in April 2020 were driven by anomalies in Europe, which had an exceptionally clear spring with record-breaking levels of solar irradiance (Madge, 2020; van Heerwaarden

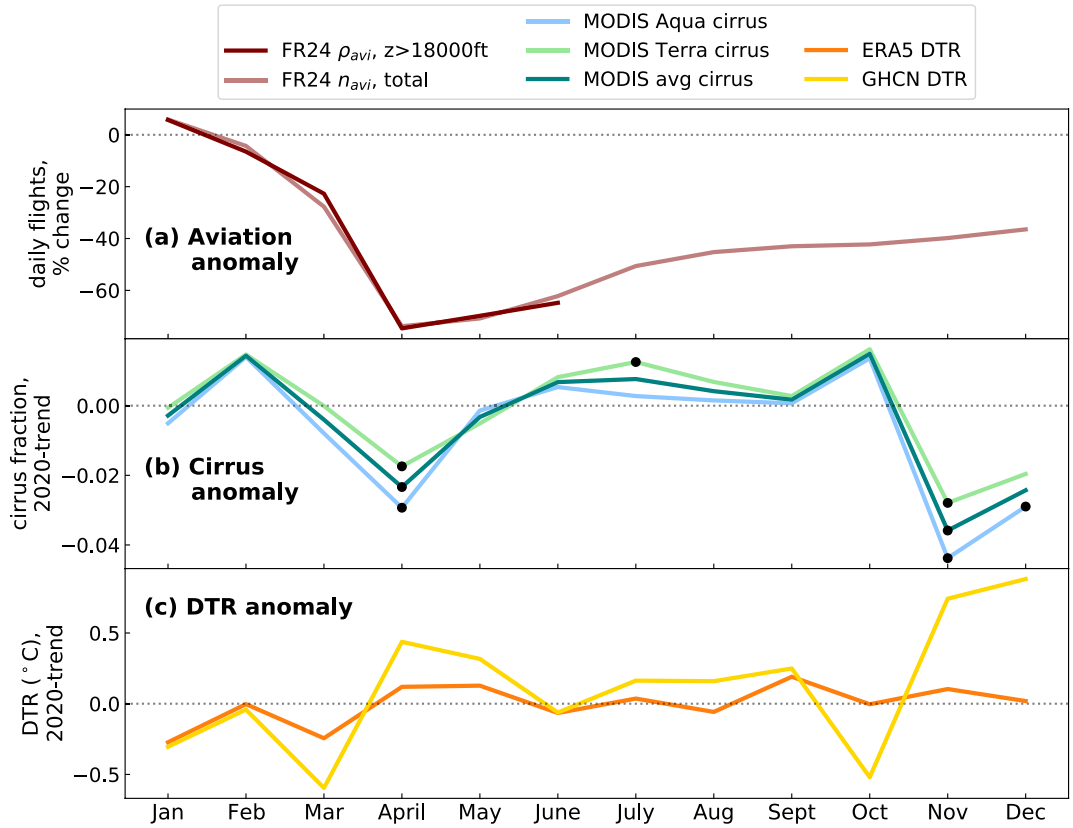

Figure 2. Monthly mean anomalies of aviation, aviation-weighted cirrus fraction, and aviation-weighted diurnal surface air temperature range (DTR) through 2020. Aviation anomalies (panel a) are expressed as a percent change over 2019 values of high-altitude aviation density and commercial flight departures (dark and light lines, respectively). The anomalies in panels (b) and (c) are expressed as an absolute change relative to a linear trend fit to the 2000–2019 values. Trends are calculated separately for each grid cell in each month. Black circles in panel (b) indicate months in 2020 where anomalies are statistically significant at the 5% level relative to their values through the reference period; significance tests were not conducted for aviation, as the anomalies are computed relative to 2019 only, and none of the DTR measurements in panel (c) were statistically significant.

et al., 2021). It has been elsewhere demonstrated that this event was not due to the reduced contrails and aerosols of the Covid-19 pandemic, but to meteorological conditions (Schumann et al., 2021; van Heerwaarden et al., 2021). Finally, joint distributions of individual grid cell anomalies (Figure S3) do not suggest dependence on aviation changes.

3.2. Comparison With Simulated Response

We next investigate whether existing simulations of AIC would predict a detectable cirrus response to the 2020 aviation reduction and whether the observed changes are consistent with the magnitude of that simulated response.

We start with a simulated global distribution of contrail cirrus coverage for the year 2006, taken from Bock and Burkhardt (2016a) (hereafter BB16). These simulations were produced using the contrail cirrus parameterization ECHAM5-CCmod, developed for the climate model ECHAM5 (Bock & Burkhardt, 2016b). Following their example, we restrict our consideration to the subset of contrail cirrus with optical depths $\tau \geq 0.05$, which has been shown to be the best threshold for comparison with satellite observations over the United States (Bock & Burkhardt, 2016a; Kärcher et al., 2009).

Only a subset of this contrail cirrus would contribute to an increase in total cirrus cover. To account for overlap with naturally occurring cirrus, we scale the BB16 contrail cirrus map by the fraction of contrail

cirrus contributing to an increase in total cloud cover shown in their Figure 6b. Since this scale factor corresponds to overlap with all cloud types, and we are interested only in the overlap with cirrus, it will tend to underestimate the simulated aviation-induced change in cirrus. We discuss the sensitivity of our results to this choice of scaling in the Supporting Information S1.

We then build a multiple linear regression model for cirrus anomalies as follows. Let $\mathbf{x}(t)$ be the annual mean cirrus anomaly field; $\mathbf{x}^{(s)}$ be the fixed simulated contrail cirrus field for 2006, scaled to account for overlap; and $a(t)$ be the aviation intensity normalized such that $a(2006) = 1$. We can then write

$$\mathbf{x}(t) = \mathbf{h_0} + c_a \mathbf{x}^{(s)} a(t) + \mathbf{h_t} t + \mathbf{w}(t) \tag{1}$$

where $\mathbf{w}(t)$ is the field of meteorological noise and $\mathbf{h_0}$, c_a, and $\mathbf{h_t}$ are fixed. If the simulated cirrus response to aviation was perfectly modeled, we would expect $c_a = 1$.

We can simplify this expression by taking the dot product of both sides with $\mathbf{x}^{(s)}$ and then dividing by the squared norm of $\mathbf{x}^{(s)}$:

$$\frac{\mathbf{x}^{(s)} \cdot \mathbf{x}(t)}{\mathbf{x}^{(s)} \cdot \mathbf{x}^{(s)}} = \frac{\mathbf{x}^{(s)} \cdot \mathbf{h_0}}{\mathbf{x}^{(s)} \cdot \mathbf{x}^{(s)}} + c_a a(t) + \frac{\mathbf{x}^{(s)} \cdot \mathbf{h_t}}{\mathbf{x}^{(s)} \cdot \mathbf{x}^{(s)}} t + \frac{\mathbf{x}^{(s)} \cdot \mathbf{w}(t)}{\mathbf{x}^{(s)} \cdot \mathbf{x}^{(s)}} \tag{2}$$

which can be written as

$$\beta(t) = c_0 + c_a a(t) + c_t t + e(t) \tag{3}$$

The term $c_t t$ (from the field $\mathbf{h_t}$) is included to account for the possibility of an unspecified linear trend due to the effects of climate change or changes in anthropogenic aerosols from nonaviation sources (Kärcher, 2017). Since we include a linear trend in our regression, we do not detrend the observed cirrus anomalies here, in contrast to the previous analyses; anomalies are simply expressed relative to the mean cirrus distribution for 2000–2019.

This model relies on two fundamental assumptions: first, that contrail cirrus production scales linearly with aviation, and second, that the spatial pattern of aviation-induced cirrus has not changed over time.

The first assumption is consistent with the findings of Bickel et al. (2020), who investigate the scaling of RF and ERF from contrail cirrus with changes in aviation density. Although they report a nonlinear response due to saturation effects at high-aviation densities, in the range of densities considered here, departures from linearity appear to be small.

The second assumption is of greater potential concern. Aviation growth has not been spatially uniform: over the period of analysis, the proportional increase of aviation in East Asia and India has been much larger than that in Europe or North America. To test the sensitivity of our results to this simplifying assumption, we conduct our analysis both for the entire globe (restricted, as above, to the range 75°S to 75°N) and for a subregion containing North America, the North Atlantic, and Europe (NAm-Eur; 130°W to 45°E, 20°N to 65°N).

The results of these analyses are shown in Figure 3. We fit Equation 3 separately for cirrus measured by Aqua, Terra, and the average of the two. We quantify aviation in terms of total kilometers flown, since this metric is the most physically relevant for contrail formation. For completeness, we repeat the analysis using the annual number of flights; these results are shown in Figure S4, and the values of c_a for all combinations of data set and domain are summarized in Table S1.

Our results indicate that, in all cases but one, the response of cirrus to changes in aviation is not statistically detectable (c_a is consistent with zero) and is considerably smaller than would be predicted from simulated contrail cirrus levels, given our assumptions ($c_a < 1$). When c_a is calculated for the Global domain using cirrus measurements from Aqua only, its result is neither consistent with zero nor with one, indicating a response that is statistically detectable but nevertheless smaller than that predicted from our model.

Our bootstrapped confidence intervals describe the expected range of meteorological variability. Had the intervals we calculate here been centered on one (i.e., had the model and assumptions described above perfectly represented the response of cirrus coverage to changes in aviation over time), none of them would intersect zero. Thus, we can conclude that these models predict a detectable signal, which does not appear in satellite observations (except, again, for in the Aqua-based calculation of a Global c_a).

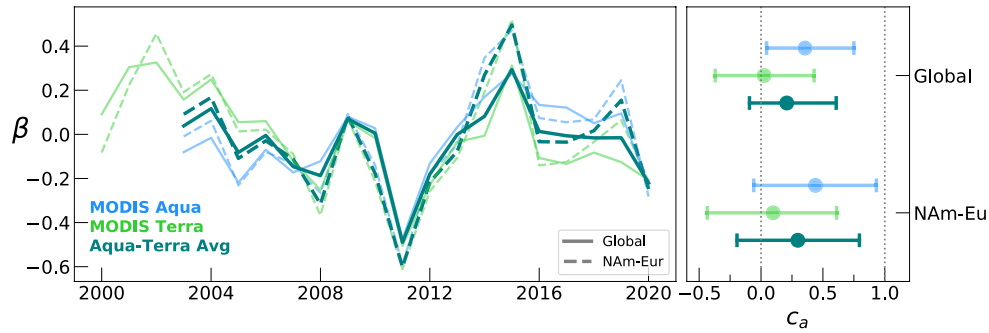

Figure 3. Lines (left panel) show the time series of β (the normalized dot product of observed cirrus anomalies on the simulated contrail cirrus pattern from Bock and Burkhardt (2016a), Equations 2 and 3). Solid lines indicate global quantities and dashed lines correspond to the NAm-Eur subregion. Points (right panel) show the regression coefficients c_a from Equation 3, with error bars spanning the bootstrapped 5–95% confidence intervals. In both panels, light-blue and light-green quantities correspond to the results obtained using cirrus measurements from Aqua and Terra, respectively; darker teal quantities are derived using the MODIS mean. The numerical values of c_a are summarized in Table S1.

Our regression model also indicates the presence of a small, and statistically insignificant, negative linear trend in $\beta(t)$ for all of the above cases. The MODIS-average predictions are $c_t = -0.01\,(-0.03, 0.08)$ and $c_t = -0.01\,(-0.03, 0.02)$ for the Global and NAm-Eur domains, respectively. We have investigated the effects of autocorrelation on the estimation of c_a and c_t and found a negligible impact on the resulting confidence intervals.

4. Discussion and Conclusions

We have investigated the response of cirrus cover and DTR to the rapid decrease in aviation that occurred in response to the Covid-19 pandemic. Neither cirrus nor DTR exhibits a response to these aviation changes which is outside the range of natural variability. Comparison with previous model simulations of aviation-induced cirrus indicates that our observations are consistent with a response which is significantly smaller than that simulated.

The absence of a detectable DTR response strongly suggests that apparent changes in DTR identified after previous much shorter and more geographically limited flight disruptions (Hong et al., 2008; Sandhu & Baldini, 2018; Travis et al., 2002) are unlikely to have been driven by changes in aviation.

We have assumed in our analysis that other (nonaviation) changes during Covid-19, such as decreases in aerosol emissions at ground level, had a negligible effect on cirrus cover. Our results could also be sensitive to the method by which we account for overlap between natural cirrus and AIC. Sensitivity analyses addressing both of these issues are described in the Supporting Information S1. They do not affect our conclusions.

Our observations have identified linear trends in cirrus coverage over the past 20 years in both aviation-weighted (Figure 1) and unweighted (Supporting Information S1) global means. These trends, which differ in sign between Aqua and Terra, are interesting in their own right and deserving of a separate, dedicated analysis beyond that which we present in the Supporting Information S1.

4.1. Comparison With Other Covid-19 Studies

Our observational nondetection of a cirrus response is broadly consistent with the results of Gettelman et al. (2021), who found the impacts of Covid-19 on high cloud to be smaller than the internal variability. However, their analysis considered annual mean quantities, and we would not expect to see a contrail cirrus response when averaged over such a long time period, given the recovery of aviation levels throughout the year. Their results are therefore not directly comparable to ours.

Schumann et al. (2021) reported that changes in cirrus optical thickness and outgoing longwave radiation over Europe in spring and summer 2020, relative to 2019, were dominated by meteorology, but that the agreement between cirrus optical thicknesses in their model and observations increased slightly when the model incorporated contrails. Although their results are suggestive of a small aviation-induced cirrus response over Europe in 2020, their simulated response may be weaker than the observed response (their Figure S1), which is opposite to our global result. Overall, their findings suggest a low signal-to-noise ratio, consistent with our results.

Finally, Quaas et al. (2021) (hereafter Q21) investigate MAM-mean changes in the Northern Hemisphere midlatitudes. They report that cirrus coverage was approximately unchanged in low-aviation regions, but decreased ~5% and 9% in the regions with the second-highest and highest 20% of air traffic, respectively. It is worth noting that these anomalies were not outside the range of the preceding 10 years' variability, except perhaps for the highest traffic region where 2020 cirrus levels appear comparable to or slightly lower than the next lowest recorded value (that from 2012). This magnitude of response is consistent with our Figure 1.

Our study primarily differs from Q21 in our methods of accounting for the high natural variability of cirrus coverage. Q21 compares the measured cirrus levels in 2020 to those in different years with similar circulation conditions; in essence, they attempt to predict cirrus occurrence using the 500 hPa geopotential height. Because of the limited sample available in the observational record and the imperfect link between 500 hPa height and cirrus, the residual changes in cirrus that they measure would still include an unknown contribution from internal variability, which is extremely difficult to characterize. To avoid this issue and ensure that the uncertainties calculated in our comparison of the simulated and modeled responses are as robust as possible, we therefore adopt the complementary approach of investigating whether observations exhibit a response that is outside the range of natural variability, comparing this response to climate simulations and using bootstrapping to estimate the uncertainty due to meteorological variability.

4.2. Implications for Radiative Forcing

A detailed assessment of the climate impacts of AIC, or of its reduction during Covid-19, is outside the scope of this work. We have exclusively looked at the changes in cirrus extent; ERF also depends on the cirrus' optical thickness (Burkhardt & Kärcher, 2011; Kärcher, 2018) and on what surface the cirrus overlays (Yang et al., 2010). Optical thickness is in turn a function of ice crystal properties (shape, size, and number) and of ambient conditions (e.g., temperature, humidity, wind shear) (Bock & Burkhardt, 2016a; Kärcher et al., 2009, 2021; Yang et al., 2010). The net effect of these properties may not be independent of cirrus coverage. However, we can make some simple inferences.

First, it is reasonable to expect that if our observations indicate a smaller response of cirrus coverage to aviation than is modeled by BB16, the resultant ERF will also be smaller.

Second, we can extend our comparison from BB16 to the current literature best estimate which was derived in the detailed multimodel synthesis of Lee et al. (2021; hereafter L21). Their assessment of the radiative forcing from contrail cirrus drew on the results from 5 global models, with corrections applied to account for differences in methodology including aviation inventory, temporal resolution, and radiative transfer scheme. Once these differences had been accounted for, the contrail cirrus ERF determined by BB16 was the smallest of those considered. Our observations are therefore consistent with an AIC ERF, which is not only smaller than that computed by BB16, but is also smaller than was found by any of the studies considered in L21.

Finally, we can use the results of BB16 and L21 to derive a back-of-the-envelope estimate for the AIC ERF implied by our observations. We emphasize that this estimate is a highly simplified approach to a very nuanced problem, and our results should not be treated as truly quantitative. A detailed description of the calculation, and of the necessary approximations involved, is provided in the Supporting Information S1. With these approximations, we find an AIC ERF of $8\,(-3, 22)\,\mathrm{mWm}^{-2}$ for 2018, well below the L21 best estimate of $57\,(17, 98)\,\mathrm{mWm}^{-2}$. Reassuringly, however, the uncertainty ranges of these two estimates do overlap.

Our results suggest that the navigational avoidance of potential contrail-forming regions is not yet a viable solution. If the ERF of AIC is indeed lower than previously believed, then the necessary increase of fossil fuel consumption caused by rerouting may result in a net increase in aviation's climate impact.

4.3. Conclusions

In conclusion, we find that observations of cirrus and DTR during Covid-19 do not exhibit a detectable response to the rapid reduction in air traffic, whereas models suggest that a cirrus response should have been detectable, despite the large natural variability of natural cirrus. Together our results imply that, although aviation influences climate through multiple processes, the cirrus-mediated effect of aviation may be smaller than previously estimated.

Data Availability Statement

This analysis utilized data from the Moderate Resolution Imaging Spectroradiometer (MODIS), hosted by NASA (https://ladsweb.modaps.eosdis.nasa.gov/archive/allData/61/ (Platnick et al., 2017)); the European Centre for Medium-Range Weather Forecasts (ECMWF) 5th Generation Reanalysis (ERA5), hosted by the Copernicus Climate Change Service (https://doi.org/10.24381/cds.adbb2d47 (Hersbach et al., 2018)); the Global Historical Climatology Network (GHCN), hosted by the NOAA National Centers for Environmental Information (NCEI) (https://www1.ncdc.noaa.gov/pub/data/ghcn/daily/by_year/ (Menne, Durre, Korzeniewski, et al., 2012)); and the CovidMIP project, available through the Earth System Grid Federation (https://esgf-node.llnl.gov/search/cmip6/). We thank these organizations for making their data publicly available. Aggregate aviation densities for 2019–20, derived from proprietary FlightRadar24 data, are available at https://doi.org/10.5683/SP2/ZGGYVO.

Acknowledgments
The authors thank Lisa Bock for making data from BB16 available and for invaluable feedback on an early version of this manuscript, and David Lee for his encouragement and generous assistance in applying the results of L21 to our work. We also thank the anonymous reviewer whose comments strengthened this manuscript. We acknowledge the support of the Natural Sciences and Engineering Research Council of Canada (NSERC) [funding reference number RGPIN-2019-04,968].

References

Airlines for America. (2021). *Airlines for America data and statistics: World airlines traffic and capacity*. Retrieved from https://www.airlines.org/dataset/world-airlines-traffic-and-capacity/

Bickel, M., Ponater, M., Bock, L., Burkhardt, U., & Reineke, S. (2020). Estimating the effective radiative forcing of contrail cirrus. *Journal of Climate*, *33*(5), 1991–2005. https://doi.org/10.1175/JCLI-D-19-0467.1

Bock, L., & Burkhardt, U. (2016a). Reassessing properties and radiative forcing of contrail cirrus using a climate model. *Journal of Geophysical Research-Atmospheres*, *121*(16), 9717–9736. https://doi.org/10.1002/2016JD025112

Bock, L., & Burkhardt, U. (2016b). The temporal evolution of a long-lived contrail cirrus cluster: Simulations with a global climate model. *Journal of Geophysical Research-Atmospheres*, *121*(7), 3548–3565. https://doi.org/10.1002/2015JD024475

Burkhardt, U., & Kärcher, B. (2011). Global radiative forcing from contrail cirrus. *Nature Climate Change*, *1*(1), 54–58. https://doi.org/10.1038/nclimate1068

Burkhardt, U., Kärcher, B., & Schumann, U. (2010). Global modeling of the contrail and contrail cirrus climate impact. *Bulletin of the American Meteorological Society*, *91*(4), 479–484. https://doi.org/10.1175/2009BAMS2656.1

FlightRadar24 (2020a). *Aviation's slow recovery: May air traffic statistics*. Retrieved from https://www.flightradar24.com/blog/aviations-slow-recovery-may-air-traffic-statistics/

FlightRadar24 (2020b). *Commercial flights down 42% in 2020*. Retrieved from https://www.flightradar24.com/blog/commercial-flights-down-42-in-2020/

FlightRadar24 (2020c). *FlightRadar24 live air traffic*. Retrieved from https://www.flightradar24.com

Gettelman, A., Chen, C.-C., & Bardeen, C. G. (2021). The climate impact of COVID-19-induced contrail changes. *Atmospheric Chemistry and Physics*, *21*(12), 9405–9416. https://doi.org/10.5194/acp-21-9405-2021

Grewe, V., Matthes, S., Frömming, C., Brinkop, S., Jöckel, P., Gierens, K., et al. (2017). Feasibility of climate-optimized air traffic routing for trans-atlantic flights. *Environmental Research Letters*, *12*, 034003. https://doi.org/10.1088/1748-9326/aa5ba0

Hersbach, H., Bell, B., Berrisford, P., Biavati, G., Horányi, A., Muñoz Sabater, J., & Thépaut, J.-N. (2018). *ERA5 hourly data on single levels from 1979 to present. Copernicus Climate Change Service (C3S) Climate Data Store (CDS)*. https://doi.org/10.24381/cds.adbb2d47

Hong, G., Yang, P., Minnis, P., Hu, Y. X., & North, G. (2008). Do contrails significantly reduce daily temperature range? *Geophysical Research Letters*, *35*(23), L23815. https://doi.org/10.1029/2008GL036108

Hubanks, P., Platnick, S., King, M., & Ridgway, B. (2020). *MODIS atmosphere L3 gridded product Algorithm Theoretical Basis Document (ATBD) and users guide*. [Computer software manual].

IATA Pressroom. (2021). *2020 worst year in history for air travel demand*. Retrieved from https://www.iata.org/en/pressroom/pr/2021-02-03-02/

Kärcher, B. (2017). Cirrus Clouds and Their Response to Anthropogenic Activities. *Current Climate Change Reports*, *3*(1), 45–57. https://doi.org/10.1007/s40641-017-0060-3

Kärcher, B. (2018). Formation and radiative forcing of contrail cirrus. *Nature Communications*, *9*(1). https://doi.org/10.1038/s41467-018-04068-0

Kärcher, B., Burkhardt, U., Unterstrasser, S., & Minnis, P. (2009). Factors controlling contrail cirrus optical depth. *Atmospheric Chemistry and Physics*, *9*(16), 6229–6254. https://doi.org/10.5194/acp-9-6229-2009

Kärcher, B., Mahrt, F., & Marcolli, C. (2021). Process-oriented analysis of aircraft soot-cirrus interactions constrains the climate impact of aviation. *Communications Earth & Environment*, *2*(1). https://doi.org/10.1038/s43247-021-00175-x

Karcher, B., Mohler, O., DeMott, P. J., Pechtl, S., & Yu, F. (2007). Insights into the role of soot aerosols in cirrus cloud formation. *Atmospheric Chemistry and Physics*, *7*(16), 4203–4227. https://doi.org/10.5194/acp-7-4203-2007

King, M. D., Platnick, S., Menzel, W. P., Ackerman, S. A., & Hubanks, P. A. (2013). Spatial and temporal distribution of clouds observed by MODIS onboard the terra and aqua satellites. *IEEE Transactions on Geoscience and Remote Sensing*, *51*, 3826–3852. https://doi.org/10.1109/TGRS.2012.2227333

Lee, D. S., Fahey, D. W., Skowron, A., Allen, M. R., Burkhardt, U., Chen, Q., et al. (2021). The contribution of global aviation to anthropogenic climate forcing for 2000 to 2018. *Atmospheric Environment*, (*244*), 117834. Atmospheric Environment. https://doi.org/10.1016/j.atmosenv.2020.117834

Madge, C. (2020). *May 2020 becomes the sunniest calendar month on record*. United Kingdom Met Office. Retrieved from https://www.metoffice.gov.uk/about-us/press-office/news/weather-and-climate/2020/2020-spring-and-may-stats

Menne, M. J., Durre, I., Korzeniewski, B., McNeal, S., Thomas, K., Yin, X., & Houston, T. G. (2012). *Global historical climatology network-daily (GHCN-daily), version 3.28*. NOAA National Climatic Data Center. https://doi.org/10.7289/V5D21VHZ

Menne, M. J., Durre, I., Vose, R. S., Gleason, B. E., & Houston, T. G. (2012). An overview of the global historical climatology network-Daily database. *Journal of Atmospheric and Oceanic Technology*, *29*, 897–910. https://doi.org/10.1175/JTECH-D-11-00103.1

Minnis, P., Ayers, J. K., Palikonda, R., & Phan, D. (2004). Contrails, cirrus trends, and climate. *Journal of Climate*, *17*(8). https://doi.org/10.1175/1520-0442(2004)017<1671:cctac>2.0.co;2

Myhre, G., Kvalevåg, M., Rädel, G., Cook, J., Shine, K., Clarke, H., et al. (2009). Intercomparison of radiative forcing calculations of stratospheric water vapour and contrails. *Meteorologische Zeitschrift*, *18*, 585–596. https://doi.org/10.1127/0941-2948/2009/0411

Platnick, S., King, M., & Hubanks, P. (2017). *MODIS atmosphere L3 monthly product. NASA MODIS adaptive processing System*. Goddard Space Flight Center. https://doi.org/10.5067/MODIS/MOD08_M3.061

Quaas, J., Gryspeerdt, E., Vautard, R., & Boucher, O. (2021). Climate impact of aircraft-induced cirrus assessed from satellite observations before and during COVID-19. *Environmental Research Letters*, *16*(6), 064051. https://doi.org/10.1088/1748-9326/abf686

Rosenow, J., Fricke, H., Luchkova, T., & Schultz, M. (2018). Minimizing contrail formation by rerouting around dynamic ice-supersaturated regions. *Aeronautics and Aerospace Open Access Journal*, *2*. https://doi.org/10.15406/aaoaj.2018.02.00039

Sandhu, A. S., & Baldini, J. U. L. (2018). Evaluating the significance of the contrail effect on diurnal temperature range using the Eyjafjallajökull eruption-related flight disruption. *Geophysical Research Letters*, *45*(23), 13090–13098. https://doi.org/10.1029/2018GL080899

Sassen, K. (1997). Contrail-cirrus and their potential for regional climate change. *Bulletin of the American Meteorological Society*, *78*(9). https://doi.org/10.1175/1520-0477(1997)078<1885:ccatpf>2.0.co;2

Schumann, U., Poll, I., Teoh, R., Koelle, R., Spinielli, E., Molloy, J., et al. (2021). *Air traffic and contrail changes during COVID-19 over Europe: Amodel study (Preprint). Clouds and Precipitation/Atmospheric Modelling/Troposphere/Physics (physical properties and processes)*. https://doi.org/10.5194/acp-2021-62

Travis, D. J., Carleton, A. M., & Lauritsen, R. G. (2002). Climatology: Contrails reduce daily temperature range. *Nature*, *418*(6898), 418–601. https://doi.org/10.1038/418601a

Travis, D. J., & Changnon, S. A. (1997). Evidence of Jet Contrail Influences on Regional-Scale Diurnal Temperature Range. *Journal of Weather Modification*, *29*(1).

van Heerwaarden, C. C., Mol, W. B., Veerman, M. A., Benedict, I., Heusinkveld, B. G., Knap, W. H., et al. (2021). Record high solar irradiance in Western Europe during first COVID-19 lockdown largely due to unusual weather. *Communications Earth & Environment*, *2*(1). https://doi.org/10.1038/s43247-021-00110-0

Voigt, C., Kleine, J., Sauer, D., Moore, R. H., Bräuer, T., Le Clercq, P., et al. (2021). Cleaner burning aviation fuels can reduce contrail cloudiness. *Communications Earth & Environment*, *2*(1). https://doi.org/10.1038/s43247-021-00174-y

Yang, P., Hong, G., Dessler, A. E., Ou, S. S. C., Liou, K.-N., Minnis, P., & Harshvardhan (2010). Contrails and induced cirrus: Optics and radiation. *Bulletin of the American Meteorological Society*, *91*(4), 473–478. https://doi.org/10.1175/2009BAMS2837.1